OPTIMIZING PRECISION OF HIGH-ANGLE ANNULAR DARK FIELD IMAGES IN SCANNING TRANSMISSION ELECTRON MICROSCOPY

A Thesis

Presented to the Faculty of the Graduate School

of Cornell University

in Partial Fulfillment of the Requirements for the Degree of

Master of Science

by

Laila Hayani

May 2018

Abstract

Scanning Transmission Electron Microscopy (STEM) is a key technique for analyzing crystal structures on an atomic scale. When fully optimized, high angle annular dark field STEM (HAADF-STEM) yields images in which atoms appear as bright spots on a dark background, making it easy to extract atomic positions quantitatively. It is crucial for us to optimize the precision of these measurements in order to be able to determine any possible atomic shifts that can arise due to the material's local properties such as ferroelectricity or charge order.

In this thesis, I investigate the limits of precision in determining atomic column positions in HAADF STEM data and how image acquisition parameters and data analysis can be optimized. In each experiment, I registered fast-acquisition stacks of $SrTiO_3$ (STO) images, determined the atomic centers in the registered images using a mixture of Gaussians for each atomic column, and finally measured the distances between each Sr column and its nearest Ti/O neighbors. Compared to previous work that required non-rigid image registration to obtain high precision from slow-scan stacks, I demonstrate that for ultra-fast scans, simple rigid registration is sufficient and precisions reached (~2-3pm) are comparable to those from non-rigid registration. Furthermore, no improvements are observed as a result of binning, nor when correcting for the scan direction with REVSTEM. I additionally compared my experimental data to simulated data with varying levels of noise added, and concluded that noise cannot possibly be the main factor in limiting my precision.

In order to reach a precision of 2-3 picometers in atomic column distance measurements, the image acquisition parameters have to be optimized. Increas-

ing stack size improved precision, though this still seems to level off around 2 or 2.5 pm. Additionally, in comparing various combinations of possible pixel densities and dwell times, I report that 1024 x 1024 x 0.25 μs/pixel scan parameters gives the best precision for typical beam currents at 300 keV and fields of view on the order of 6.6 nm.

Although some of these experimental parameter changes did improve the precision, none of my data sets were able to get a precision in the Sr-Ti/O column distances in $SrTiO_3$ below 2 pm, indicating that there is some underlying systematic process that limits my precision. Future experiments performed on different samples or at cryogenic temperatures could determine if this issue is due to the microscope setup or due to a physical shift in the lattice itself.

Biographical Sketch

Laila Hayani was born and raised in the suburbs of Chicago, IL to Ammar and Karen Hayani. Since her beginning days, she was always interested in math and science, and had planned to pursue medicine as a career. She did her undergraduate studies at Northwestern University, where she double major in Biological Sciences and Religious Studies. But, after working at Abbott Laboratories for a year, she decided to change fields and pursue a career in applied and engineering physics, at which point she enrolled at Cornell University for a Master of Science.

Upon completion of her M.S., she plans to begin a Ph.D. program at the University of Michigan, Ann Arbor. She hopes to conduct research on technology for renewable energies that will reduce our carbon footprint. In her spare time, Laila can be found advocating for social and environmental justice, skyping with her college roommates, or playing roller derby with the Ithaca League of Women Rollers.

Acknowledgements

Bismillah al-Rahman al-Rahim

There are countless people who have supported me on my journey and whom I could not have gotten here without.

I would like to first and foremost thank my advisor, Dr. Lena F. Kourkoutis, for taking me on as a student in her lab and introducing me to the world of electron microscopy. She has been extremely supportive in my research and has always pushed me to think about my research in new and exciting ways.

I'd also like to thank Dr. Brock for being on my special committee and serving as my advisor since I first arrived on campus. His guidance in navigating a new environment and program of study has been invaluable.

I'm extremely grateful to all of my professors, who have excited me about various fields of physics, and have made my classes fulfilling and engaging. Special thanks to Prof. David Muller and Prof. Frank Wise for piquing my interest in quantum mechanics.

I'd also like to thank all of the students in the Kourkoutis lab who have patiently helped me in learning about electron microscopy from scratch. Special thanks to Berit Goodge for teaching me all about STEM and helping me troubleshoot experiments, in addition to taking data on the Titan Transmission Electron Microscope. Additional thanks to Ismail El Baggari and Benjamin Savitzky for their help in python coding, and to Colin Clement for his MOG code.

Of course, my time at Cornell wouldn't have been the same without the love and support of my friends who made my time here so valuable. To Mishcat, Aneesa, Mahfuza, and Tarannum for always making me feel at home. To Ibti-

saam, who has been my moral support through all of this and who inspires me to follow my own path wherever it leads me. And to Alaa for being my role model and always supporting me despite the distance.

Finally, I would like to thank my family, for I would not be where I am today without them. To Kinan, Meredith, Zayd, and Samar for their endless love and support. And of course, to my parents for raising me to be the woman I am today, for cultivating my interest in math and science since childhood, and for supporting me in my non-medical career.

Contents

List of Figures

Chapter 1

Introduction

1.1 Introduction to Electron Microscopy

Light microscopy has been around since the 17th century, with some of the earliest compound microscopes used to look at biological specimens. The Dutch biologist Antonie van Leeuwenhoek was able to create a compound microscope that could resolve as small as one micron, but chromatic and spherical aberrations created problems for image clarity and limited the microscope's resolving power. As decades and centuries passed, scientists developed aberration corrections that improved the resolving power of these compound optical microscopes [16]. But in 1873, German physicist Ernst Abbe discovered that optical microscopes were inherently limited not by the quality of the instrument, but rather by the wavelength of visible light. He found the diffraction limit to be

$$d = \frac{\lambda}{2NA} \tag{1.1}$$

where d is the minimum resolvable distance between two objects, λ is the wavelength of light used to image the objects, and NA is the numerical aperture of the lens [5]. Since visible light has wavelengths of approximately 400-700 nm, this would mean that optical microscopes could not resolve distances much less than about 200 nm.

Thus, the need for the electron microscope emerged. Louis de Broglie theorized the wave-like properties of electron beams, and that their wavelength could

be tuned by their energies, similar to photons. If the energy of an electron is relativistic, then the wavelength of the electron beam is

$$\lambda = \frac{h}{p} = \frac{hc}{E} \tag{1.2}$$

where E is the energy of the beam, h is Planck's constant, and c is the speed of light [13]. In this thesis, I use electron beam voltages of 300 keV to resolve $SrTiO_3$ (STO) lattices. At this energy, the electron beam will have a wavelength of 4.13 pm, allowing for imaging of atomic structures that are on the order of a few angstroms.

1.2 Scanning Transmission Electron Microscopy

In this thesis, I use a specific mode of electron microscopy known as Scanning Transmission Electron Microscopy (STEM), depicted in Fig. 1.1. In STEM mode, an electron beam is focused onto a point on a sample and is then scanned through the sample like an ink printer. The sample must be electron transparent (on the order of tens of nanometers thick) as well as be aligned so that the atomic columns are parallel to the axis of the beam. When the electron beam is focused to the position of an atomic column, the electrons will be elastically scattered to a high angle off the axis, shown in Fig. 1.1 as the purple conical region. These electrons will be captured by a high-angle annular dark field (HAADF) detector. Atomic columns will show up as bright spots on a dark background [21].

When the electron beam is focused onto an interstitial point in the crystal lattice, the electrons are able to channel in this space between the nuclei, and are therefore deflected to a small angle. This is shown in Fig. 1.1 as the translucent blue region that is concentric with the purple HAADF region. These electrons will be captured by the annular bright field (ABF) detector. Atomic columns will appear dark on a bright background [21].

In both ABF and HAADF imaging, the brightness of the atomic column has

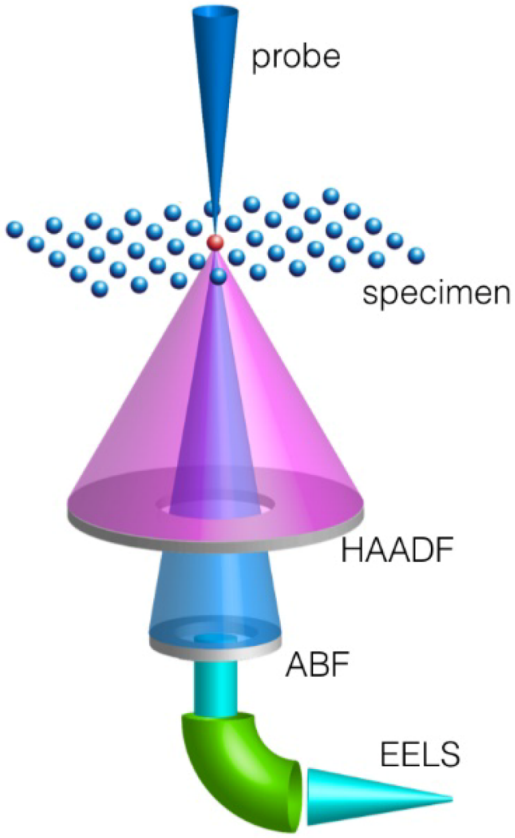

Figure 1.1: Scanning Transmission Electron Microscopy (STEM) mode of the Titan. An electron probe scans through the sample row by row. The electron beam will deflect to a higher angle when the probe is directly over an atomic column than when the probe is between atomic columns. Image Source: [20]

a high Z-dependence, where Z is the atomic number. In ABF images, strontium columns appear larger and darker than titanium/oxygen columns. In HAADF images, strontium columns appear larger and brighter than titanium/oxygen columns. However, it is important to note that light atoms, such as oxygen, are only visible in ABF and not in HAADF; they are not heavy enough to scatter the electron beam to high angles at a measurable level [21].

In this thesis, I solely analyze HAADF data because they are less sensitive to issues such as sample tilt [12]. This makes them more robust for the purposes of studying limits of precision.

1.3 Motivation for Improving Precision

Obtaining images with high precision is extremely important for atomic-scale research. Physicists need to be able to precisely identify the locations of atomic columns in HAADF images if they are to study slight atomic shifts in the material. These shifts are often on the order of a few picometers and can be the result of effects such as lattice distortions and strains in the material.

For instance, in crystal perovskites, charge density waves introduce picometer-scale periodic lattice displacements (PLDs), and are important for studying metal-insulator transitions and superconductivity [2]. Previous research has shown perovskites such as $Bi_{0.35}Sr_{0.18}Ca_{0.47}MnO_3$ (BSCMO) to display PLDs that are less than 10 pm, due to these charge density waves [18].

Apparent picometer-scale shifts of atomic columns in STEM images can also arise from experimental errors in imaging, such as small tilts in the sample itself. ABF images are especially sensitive to sample tilt, demonstrating atomic column shifts of a few picometers when the sample is tilted by a few milliradians [23]. Although the HAADF images I analyze in this thesis would be less sensitive to these sample tilts, understanding the limits of precision for HAADF could possibly improve the precision of ABF images by identifying optimal acquisition parameters as well as data analysis tools.

1.4 Improving Signal-to-Noise with Registration

In order to extract high precision information about atomic positions from HAADF-STEM images, a high signal-to-noise ratio is needed. For atomic resolution images, this implies that the signal on an atomic column needs to be maximized. In counting statistics, the noise of a pixel in an image is given by $\sqrt{N}$, where N is the total number of counts in the pixel. To get a high signal-to-noise ratio, we need the number of counts to be as large as possible. This then allows us to locate low-intensity atomic columns in addition to being able to distinguish atoms with

similar atomic numbers [15]. Furthermore, the ability to definitively distinguish atomic columns from the background is crucial for correctly identifying the center of each of these atomic columns. If the signal-to-noise ratio of an image is low, the fitting to each atomic column will have a much higher uncertainty, which decreases precision down the line of our analysis. The error in locating the center of any atomic column should be as low as possible if we are to study any physical or chemical properties of a material [1].

With this in mind, there are two options for obtaining a high signal-to-noise ratio image for a chosen beam current. First, the microscope can obtain a large number of counts by scanning through the region of interest in a single scan but do so slowly on the order of a few to tens of seconds per scan. However, this is an issue when the image is completed. As the HAADF-STEM scan in Fig. 1.2 shows, by the time the electron probe reaches the end of the scan, the entire lattice has shifted by a significant amount, resulting in a distorted image [1, 4, 17].

Therefore, we use our second option in getting a high signal-to-noise ratio: taking multiple fast scans and registering them together. If each scan takes less than a second, then the atomic columns have not moved much in the time it takes to complete a scan, and any scan distortions will be minimized in the final image. Each scan has a low signal-to-noise ratio, but this would be alleviated by registering the images together to create a correlated image with a large number of total counts and a high signal-to-noise ratio [19].

A variety of registration methods have been used in a range of scientific fields including medical imaging and radar imaging. These registration methods rely on detecting features in an image, matching the features from one image to the next, and creating a transformation map between the two images [24]. In STEM, there are two main methods of registering a stack of HAADF scans to create a correlated image, and they are described in detail in the following two subsections.

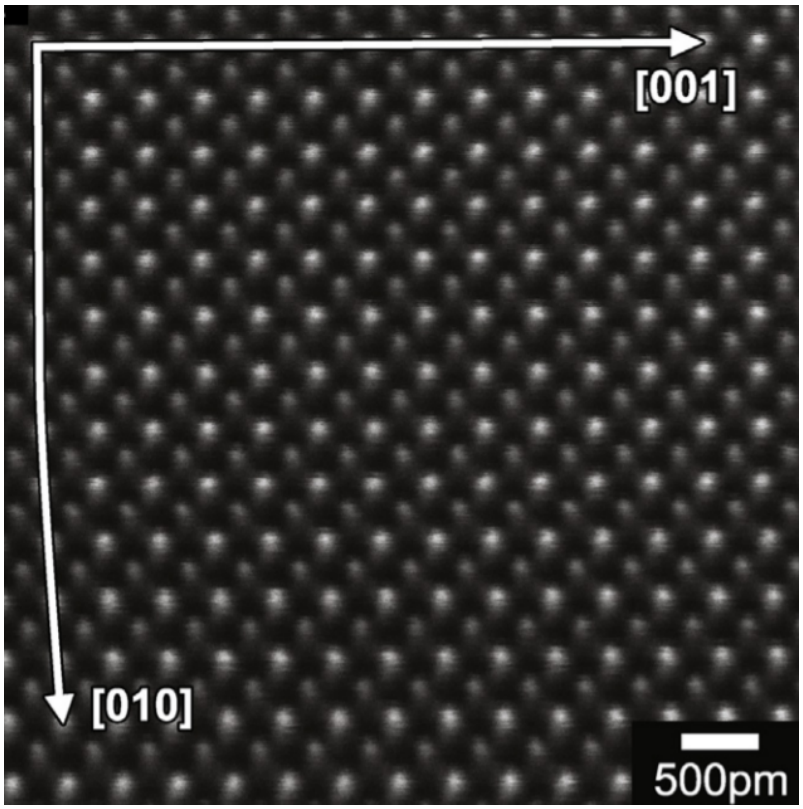

Figure 1.2: HAADF-STEM image of $SrTiO_3$ with high signal-to-noise but distorted lattice due to a long scan time. As the microscope probe moves from the top to the bottom, the sample shifts to the right, and the lattice axes become distorted. Image Source: [17]

1.4.1 Rigid Registration

Of the two methods, rigid registration is the more conceptually simple. It assumes that all the atomic centers in the image shift by the same amount and in the same direction from one frame to the next. Even though this neglects any small amounts of scan distortions that might happen over the course of a single scan, it is a very good first order approximation for fast scans. The code uses these shifts to relate each image in a stack to every other image in the stack, and can now correlate these images together to create a single image with a high signal-to-noise ratio [19]. This method is demonstrated in Fig. 1.3, and is discussed in greater detail in Section 2.1 of this thesis.

The method of rigid registration I used in this thesis is the one developed by my former labmate Dr. Benjamin Savitzky. This technique was developed primarily for low signal-to-noise cryo-STEM data in which fast scans must be

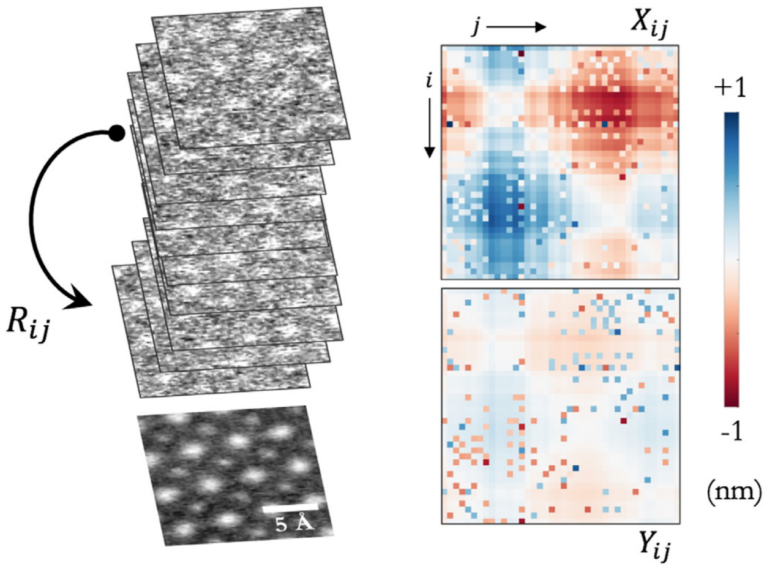

Figure 1.3: Overview of rigid registration. Left: each image in a stack is related to every other image in the stack by a rigid translation. Right: a shift matrix ($R_{ij} = X_{ij}\hat{x} + Y_{ij}\hat{y}$) is created to show the translations between every combination of images (i,j) in the stack. Image Source: [19]

taken [19], but is still applicable for the data sets here due to their fast frame times.

1.4.2 Non-rigid Registration

On the flip side, non-rigid registration takes into account lattice shifts within a single frame. It does not assume that each image in a stack is uniformly shifted in comparison to other images in the stack. Instead, it allows for distortions due to sample drift and probe instabilities to be taken into account, as shown in Fig. 1.4 [22].

The non-rigid technique developed by Berkels et al. [4] and Yankovich et al. [22] takes two frames and maps them onto a common transformed, nonparametric coordinate system. This non-rigid registration works on a multilevel scheme, starting with coarse alignment among the images, and then is done again with a finer level of resolution. This fit is optimized on multiple levels using gradient flow to minimize displacements between each set of images. Once this is done, all of the frames can be mapped back onto a single reference frame.

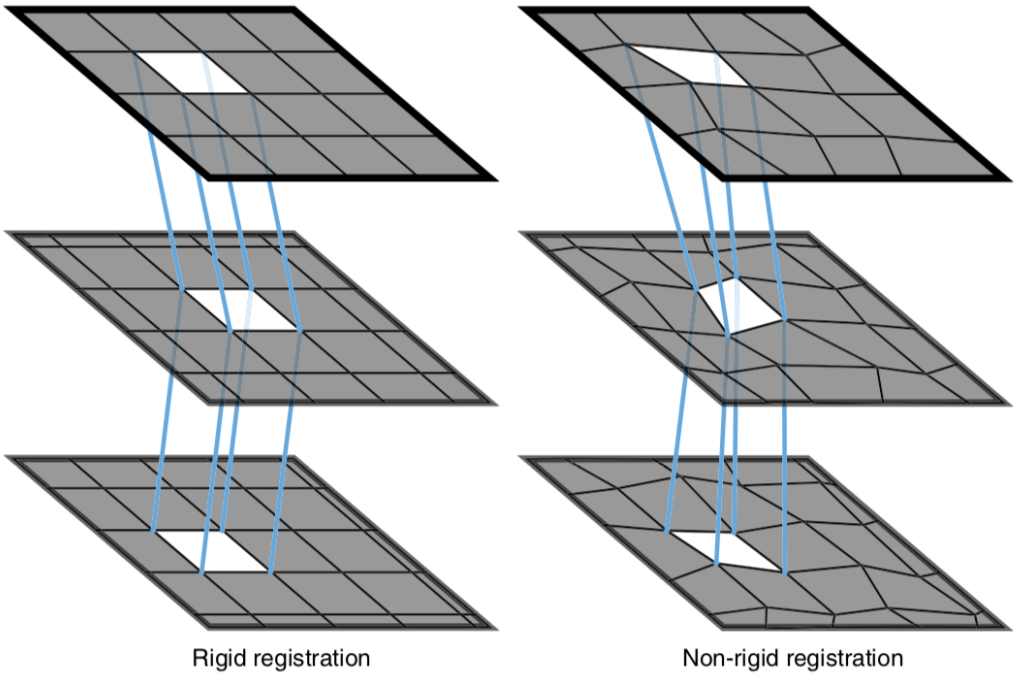

Figure 1.4: Comparison of rigid and non-rigid registration methods. Rigid registration assumes that all atomic coordinates are shifted by the same amount and in the same direction from one image to the next. Non-rigid registration allows for distortions in the image to be taken into account when tracking a feature from one image to the next. Image Source: [22]

1.5 Previous work on precision

A plethora of previous research has been done to push the limits of precision to lower and lower values. Kimoto et al. [15] demonstrated 5 pm precision in annular dark field (ADF) imaging of $TmFeO_3$, which corresponds to about 1% strain in the crystal structure. They measured precision by comparing atomic positions to their expected translationally symmetric positions. Kim et al. [14] measured lattice spacings in $La_{0.5}Sr_{0.5}CoO_{3-\delta}$ (LSCO) ADF-STEM data with an standard deviation of ±4 pm, citing this as the precision of the image.

Yankovich et al. [22] was able to achieve sub-picometer precision in measuring atomic spacing in Si by non-rigidly registering HAADF-STEM images. They acquired a stack of 512 images of Si in the [110] direction with 256 x 256 pixels and 13 μs/pixel dwell time. They then registered this image stack both rigidly and non-rigidly and found that the rigidly registered image achieved a precision

of about 4-5 pm, while the non-rigidly registered image achieved sub-picometer precision.

Other researchers have also improved precision by minimizing scan distortions. Xiahan Sang and James M. LeBeau [17] developed a technique called Revolving STEM, or REVSTEM, in which the direction of the scan is rotated by 90° every scan. They measured Sr-Sr and Ti-Ti distances in a REVSTEM image of STO with a 1024 x 1024 pixel frame size and a 5 μs/pixel dwell time. They plotted the histograms of these distances for first like neighbors (FLN) and second like neighbors (SLN), and cited the standard deviations of these histograms as precisions of 1.5 pm and 2.4 pm respectively.

In this thesis, I analyze HAADF-STEM image stacks comprised of fast scans (0.5 μs/pixel) to determine how to improve the precision of these images, and to gain insight as to what are the experimental or analytical factors that limit precision of these images.

Chapter 2

Methods

2.1 $SrTiO_3$ Lattice Structure

In this thesis, I use $SrTiO_3$ (STO) to study precision because its cubic lattice structure makes it easy to measure atomic column distances. There should be no periodic lattice displacements in STO, so the bond lengths should be consistent across the entire HAADF image. The lattice constant for STO is 390.5 pm [6]. Because Ti/O columns are evenly spaced in the center between Sr columns, this means that the distance between a Sr column and a Ti/O column should be approximately 276.125 pm. I took STEM data of thin STO samples in order to analyze the precision of these Sr-Ti/O atomic column distances.

2.2 Registration

For registering the images, I primarily used Dr. Benjamin Savitzky's rigid registration code [19]. The code takes a stack of fast scan STEM images and compiles them into a single registered image with a high signal-to-noise ratio, as shown in Fig. 2.1.

First, the rigid registration code applies a Fourier mask to every image in the stack in order to eliminate high-frequency noise information, leaving only low-frequency information from the lattice. This allows for the code to more precisely register images in the stack. The code then creates a shift matrix that relates the shifts between each image and every other image in the stack. The shift matrix is

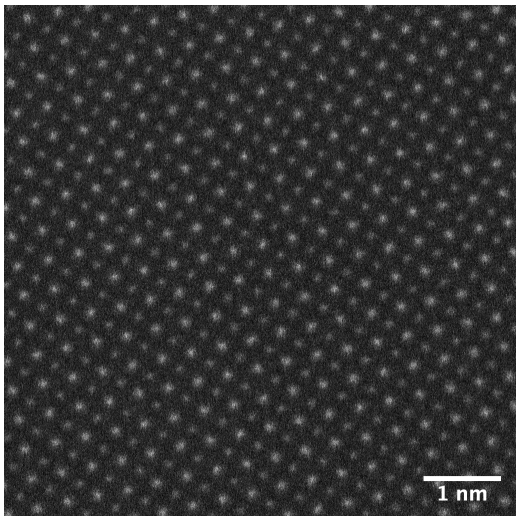

(a) A single fast scan in a stack of 20 images

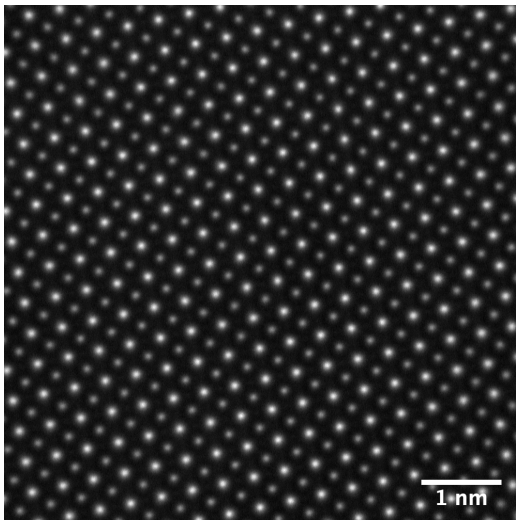

(b) The final registered image with a high signal-to-noise ratio

Figure 2.1: Rigid registration allows for a stack of many fast scans with low signal-to-noise ratios to be correlated into an image with a high signal-to-noise ratio.

expected to have a smooth background, as seen in Fig. 1.3, which is indicative of the stage drift of the sample over the time it takes to acquire an entire stack. The background is expected to be smooth because each scan in a stack should be only slightly shifted from the previous and following scans. There are also typically a few outliers that can be identified by eye because of their breaking with the smooth background, as seen in Fig. 2.2a. These outliers can be identified by the rigid registration code by enforcing additive transitivity within the matrix. This means that any value in the matrix should be able to be calculated from the sum of two other points in the matrix. For example, if we know the shift from image 1 to image 5 and from image 5 to image 10, then we can use the sum of these shifts to determine the correct shift from image 1 to image 10. Any values in the matrix that do not obey this transitivity are labeled as outliers in the matrix, shown in Fig. 2.2b. The matrix is then corrected by forcing these outlier points to follow additive transitivity with the rest of the matrix. This yields a smooth shift matrix, such as the one in Fig. 2.2c, which can then be used to create a registered image with a high signal-to-noise ratio [19].

Fig. 2.2 shows the shift matrices for the displacements in x for a stack with 20

fast scans. Similar shift matrices are also generated for shifts in y. The registered image generated from this matrix, such as the one shown in Fig. 2.1b, is used in analyzing atomic column positions in this thesis.

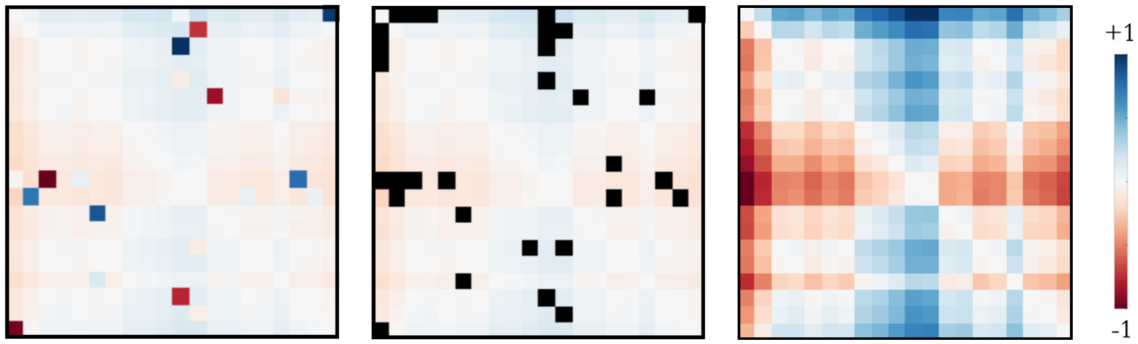

(a) Uncorrected shift matrix

(b) Shift matrix with outliers in black

(c) Corrected shift matrix

Figure 2.2: Shift matrix of the displacements in x. Left: each image in a stack is cross-correlated with every other image in the stack to determine their relative shifts, yielding a shift matrix. The shift matrix is normalized on a scale of -1 to +1, shown by the color bar on the right. Center: the rigid registration code determines the outliers of shift matrix based on transitivity. Right: the matrix is then corrected and used to correlate the image into a single image with a high signal-to-noise ratio.

2.3 Atomic Tracking

After creating the registered image with Savitzky's rigid registration code, I needed to accurately determine the positions of atomic columns and their distances from one another. I first used the Photutils package to identify bright two-dimensional Gaussians in a dark background to a relatively good accuracy [10]. Then, I ran these coordinates through another code which optimizes them to a higher accuracy using a mixture of Gaussians (MOG) [7]. Finally, I used these coordinates to calculate the distances between neighboring atomic columns.

2.3.1 Photutils

Photutils is a python package within the Astropy [11] project for astronomy-related python softwares. It can be used for detecting stars in astronomical images. Here, I used Photutils for finding the centers of each atomic column. The

code takes the registered STEM image and searches for local maxima above a given threshold. It then uses a two-dimensional Gaussian, determined by an input parameter for the full width at half maximum (FWHM), to find the center of the atomic column [10]. The FWHM was determined by estimating the radius of the Sr atomic columns in the registered image. The output of the Photutils code is a two-dimensional matrix with coordinates for each atomic column [10]. The FWHM has to be adjusted for each image based on its magnification so that the code can locate atomic column positions correctly.

2.3.2 Mixture of Gaussians (MOG)

Photutils uses a fixed FWHM for fitting a 2D Gaussian to each atomic column in the image [10], but in reality, the FWHM of a Sr atomic column would be larger than the FWHM of a Ti/O atomic columns. Therefore, I still needed to optimize these coordinates in a more robust fashion if I want to obtain picometer-level precision. I used a code that optimized these coordinates by fitting a 2D Gaussian to each atomic column separately. A code developed by Colin Clement for the purpose of analyzing STEM images takes the rough inputs from Photutils and uses a mixture of Gaussians (MOG) at each of these coordinates to determine the atomic position and size [7]. Depending on the signal-to-noise ratio and distortions of the image, the MOG code takes several to tens of minutes to find the optimized centers. Though this process takes a while, the MOG output typically returned an uncertainty of fit under 1.5 pm for each atomic column, with better fitting for images with higher pixel densities. A sample of the visual output of the MOG fitting is shown in Fig. 2.3. It is also important to note that with both Photutils and MOG, the atomic coordinates are not forced to be in the center of a pixel.

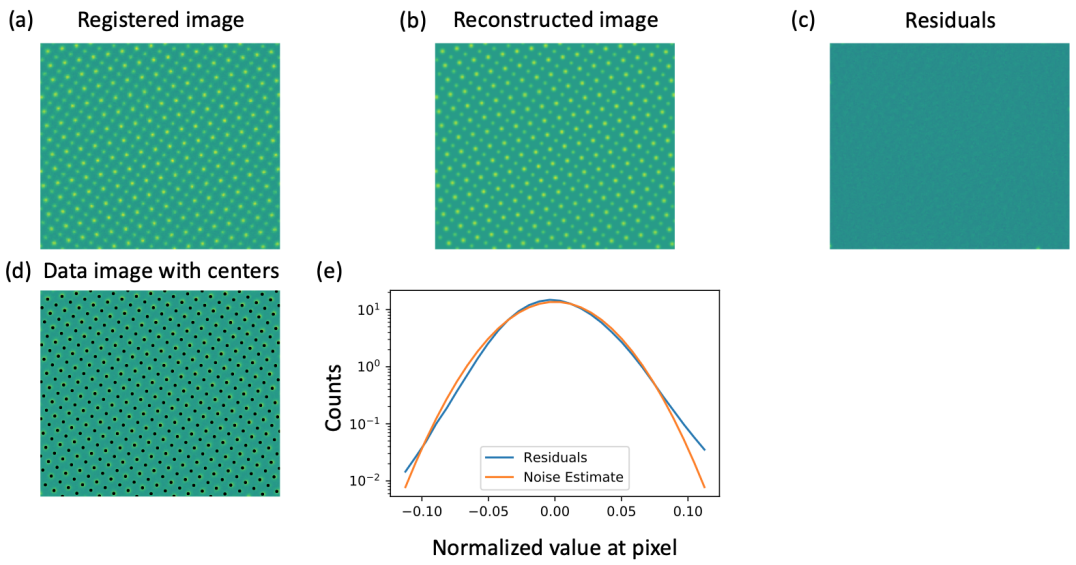

Figure 2.3: MOG fitting results. **(a)** The registered experimental image is normalized so that the maximum value of a pixel can be 1. **(b)** The code determines the size and position of Gaussians for each atomic column and creates a reconstructed image using this information. **(c)** The residuals are the difference between the registered image and reconstructed image. A low residual map shows that the fit is good. **(d)** The data image is shown with the centers found from the MOG fitting. **(e)** The level of noise in the image is estimated and plotted to compare to the residuals.

2.3.3 Determining Atomic Column Distances using the Nearest-Neighbor Method

Once I obtained the positions for atomic columns, I needed to determine the precision of the distance from each Sr column to the four closest Ti/O columns.

First, I separated the coordinates based on atomic type. I ran the registered image through Photutils again but this time with higher threshold to select for only Sr atomic columns since these are brighter than Ti/O. Coordinates from the MOG output that are within a few pixels of these new Sr coordinates are labeled as Sr atoms in a boolean matrix.

I then eliminated atomic coordinates that were closest to the edge of the image. If the FWHM input is greater than the distance between a given atomic center and the edge of the image, then the atomic column would be cut off by the edge of the image. This makes the calculated center of these atomic columns unreliable.

In order to determine the four nearest Ti/O neighbors to each Sr column, I used the KDTree class of the Scipy python package. KDTree is an algorithm that creates a binary tree for an array of coordinates, which can then be queried to find the four nearest neighbors to every coordinate in the array [9]. Using the indices of each of the four nearest neighbors to a given atomic column, I found the distances between Sr atomic columns and their neighboring Ti/O columns, which should be around 276.125 pm. For atomic columns near the edge of the image, some of the nearest neighbors found by KDTree were an extra lattice period away, giving a Sr-Ti/O distance of around 600-800 pm (depending on the geometry). In order to eliminate these incorrect nearest neighbors from my analysis, I discarded values from the data set that were greater than 350 pm. I chose this value as the cutoff value so as to ensure that there was ample leeway for any abnormally large Sr-Ti/O atomic column distances while also excluding any distances greater than one lattice period away.

To account for the differences in Sr-Ti/O distances due to scan direction, I separated each of these distances according to the angle created by the Sr-Ti/O line drawn, as shown in Fig. 2.4. I then created histograms of the distance measurements at each of these angles: $\pi/4$, $3\pi/4$, $-\pi/4$, and $-3\pi/4$. Following the definition of precision used by Yankovich et al. [22] and Bals et al. [3], the precision for Sr-Ti/O distances in a given direction is determined by the standard deviation of the corresponding histogram. The overall precision of the image is from the composite of Sr-Ti/O distances in all four directions.

2.4 Definition of Uncertainty of Gaussian Fit vs. Precision of Atomic Column Distances

There are two ways to define the precision of HAADF-STEM images that I use in this thesis: uncertainty of MOG fitting and precision of Sr-Ti/O atomic column distances.

If atomic columns are well separated in an image, then I can estimate the

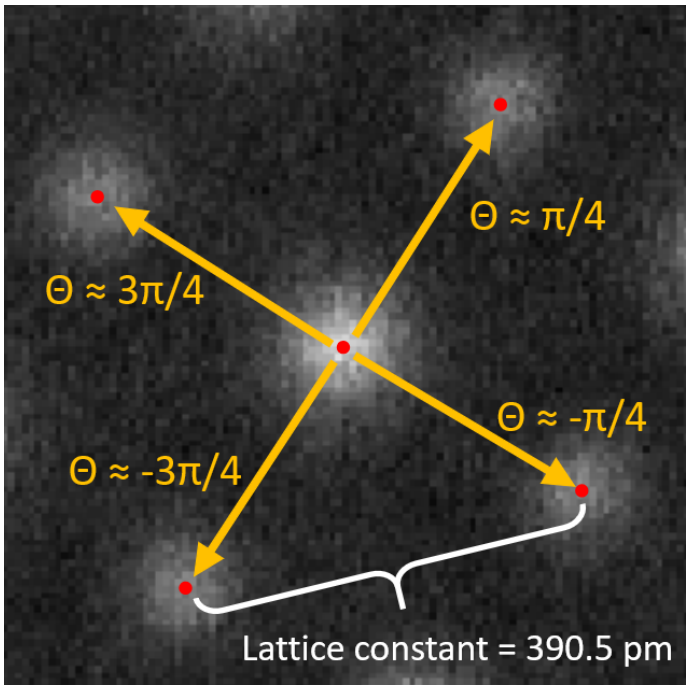

Figure 2.4: Sr atom (center) with nearest Ti/O neighboring columns found by KDTree. Arrows from Sr to Ti/O represent the distances found, which are used to determine precision of the image, separated out by directions as shown.

uncertainty in the localization of their centers. For each atomic column, the MOG code returns an uncertainty of the fitting procedure, typically less than 1.5 pm. This means that the true center of the atomic column is likely to be within this distance from the reported coordinate of the atomic column [7]. For this thesis, I will call this the MOG fitting uncertainty.

However, defining the precision of an image as a whole cannot be done by only looking at the uncertainty of the fitting to each atomic column. If we scan across a sample to take an image rather than taking a snapshot of it, we need to account for changes during the scan, such as the distortions shown in Fig. 1.2. This is especially important for slower scans, where the fitting to each atomic column could be excellent while the image as a whole shows a clear distortion of the lattice. Therefore, I use the definition of precision used by many other microscopists, which is the standard deviation of the distances between atomic columns and their nearest neighbors [3, 17, 22].

2.5 Experimental Details

All HAADF-STEM images in this thesis were taken with a Titan transmission electron microscope using a beam voltage of 300 keV, a convergence angle of 21 mrad, and a magnification of 14.5 MX. For each image, the pixel size in picometers was calibrated by taking a fast Fourier transform (FFT) of the registered image and measuring the distance in pixels from the central peak to the Bragg peaks at (200) and (020). This distance corresponds to half of the lattice constant. I used the secondary Bragg peak rather than the primary ones because their centers were the easiest and most reliable to locate. I then averaged over all four secondary Bragg peak distances and divided the half-lattice constant by this value to get the pixel size in picometers, shown in the following equation,

$$\frac{390.5/2}{a} = \frac{\text{x pm}}{\text{pixel}} \tag{2.1}$$

where a is the average distance from the center of the FFT to the secondary Bragg peaks, and x is the size of a pixel in picometers.

Chapter 3

Results

3.1 Non-Rigid vs. Rigid Registration

Choosing between a non-rigid or rigid registration can have an effect on the precision in the image, as demonstrated by Yankovich et al [22]. I compare our group's rigid registration to the non-rigid registration developed by the Voyles research group by running one of my data sets through each registration code. I used a 1024 x 1024 pixel data set with 0.5 μs/pixel dwell time.

Both the non-rigidly registered image and the rigidly registered image were given the same input parameters for Photutils and MOG optimization. The uncertainty in MOG fitting of each atomic column was approximately the same between the two images. For each image, I averaged the uncertainties of each atomic column to give an average MOG fitting uncertainty for the entire image. This yielded an average MOG fitting uncertainty of 0.32 pm for both the non-rigidly registered and the rigidly registered images. This indicates that the Gaussian fitting around each atomic column is unaffected by the registration method.

In comparing the distribution of Sr-Ti/O distances for each image, the precisions between the two methods were approximately the same. Although I had hoped that non-rigid registration would help me to achieve sub-picometer precision as it did in the article by Yankovich et al. [22], this was not the case for this data set and for these parameters. I show in Fig. 3.1 the histogram for Sr-Ti/O distances at an angle of $\pi/4$ from the Sr column. For the distances at $3\pi/4$, -$\pi/4$, and -$3\pi/4$, the respective values of precision for rigid registration are 2.67 pm,

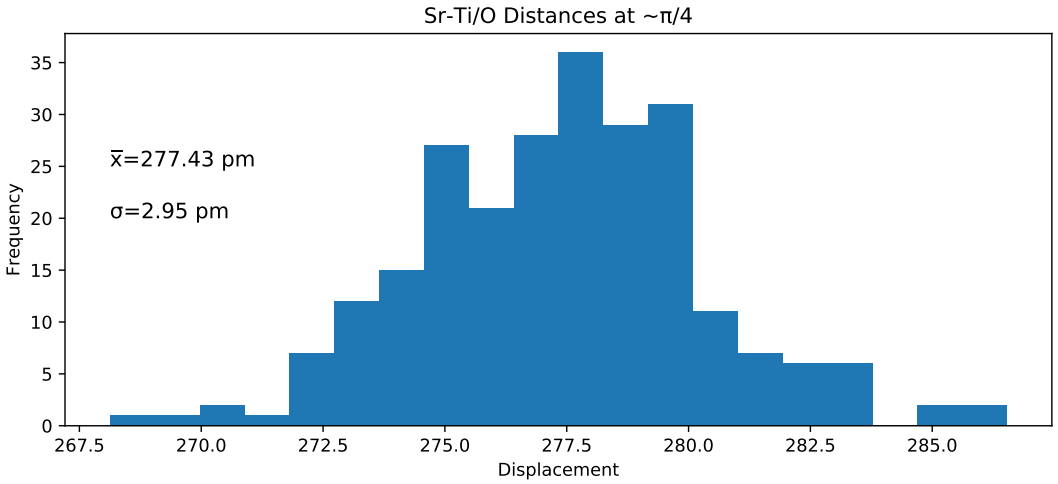

(a) Rigidly registered image

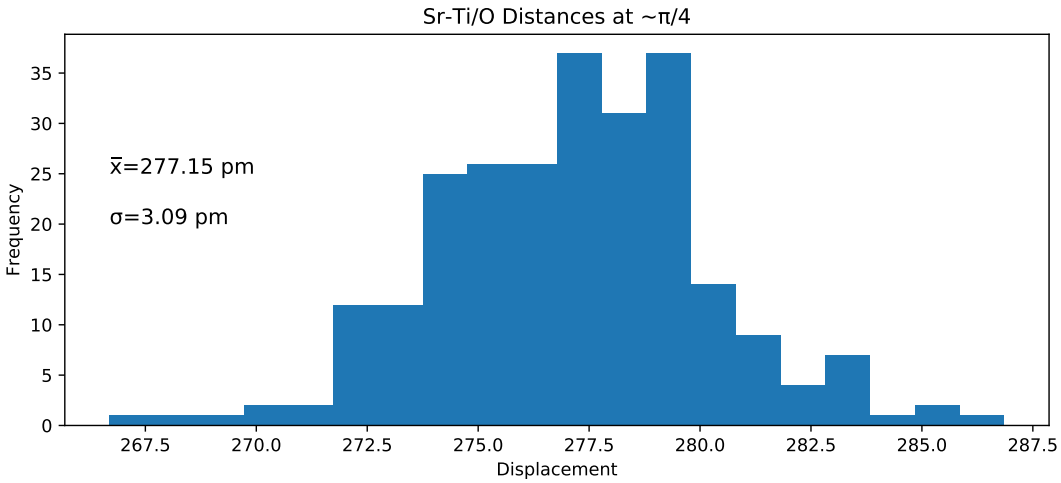

(b) Non-rigidly registered image

Figure 3.1: Comparison of precisions for rigidly registered and non-rigidly registered images in direction of $\pi/4$. Precisions of rigid compared to non-rigid Sr-Ti/O distances are approximately the same for each of the four directions.

2.56 pm, and 2.90 pm, and for non-rigid registration are 2.79 pm, 2.48 pm, and 2.86 pm.

However, it is not a general statement to say that rigid registration universally gives similar precision to non-rigid registration. This was only tested on one data set, and it is important to note that each registration technique is optimized for different scan parameters. Savitzky's rigid registration code is optimized for STEM data with short pixel dwell times, giving each individual image a low signal-to-noise ratio [19]. The Yankovich non-rigid registration, however,

is optimized for images with longer scan times. The data set used by Yankovich et al. to show sub-picometer precision had scan parameters of 256 x 256 pixels with 13 μs/pixel dwell time, giving a total frame time that is nearly double that of my frame time. Longer frame times make scan distortions within a frame more prevalent, calling for the need for non-rigid registration and leading to lower precision if done with rigid registration [22].

3.2 Correcting for Scan Direction (REVSTEM)

I additionally checked for the affect of scan distortion on precision by using a technique called Revolving Scanning Transmission Electron Microscopy (REVSTEM), developed by Xiahan Sang and James M. LeBeau [17]. In this technique, I acquired a 1024 x 1024 x 0.5 μs/pixel stack in which the scan direction is rotated by 90° midway through every other scan. Image slices for which the scan was rotated halfway through were deleted from the stack, and all other image slices were rotated back to the original orientation. I then registered the stack, found the optimized centers using the MOG, and determined the distances between atomic columns.

The total uncertainty in MOG fitting was 0.43 pm, and the precision of the atomic column distances averaged over the entire image was 3.39 pm, as shown in Fig. 3.2. This is comparable to the precision values I have cited for non-REVSTEM images. Because these scans are fast, not much sample drift happens in the time that a single scan is performed, so scan distortion is minimal. This is in agreement with my comparison of non-rigid vs. rigid registration methods, where scan distortion doesn't seem to be a significant factor in limiting precision.

I can conclude that when using these scan parameters (specifically fast scans), averaging out the scan distortions related to scan direction do not improve the precision of my images. Therefore, it must be a different physical phenomena that creates variations of atomic distances and keeps my precision above 2 pm.

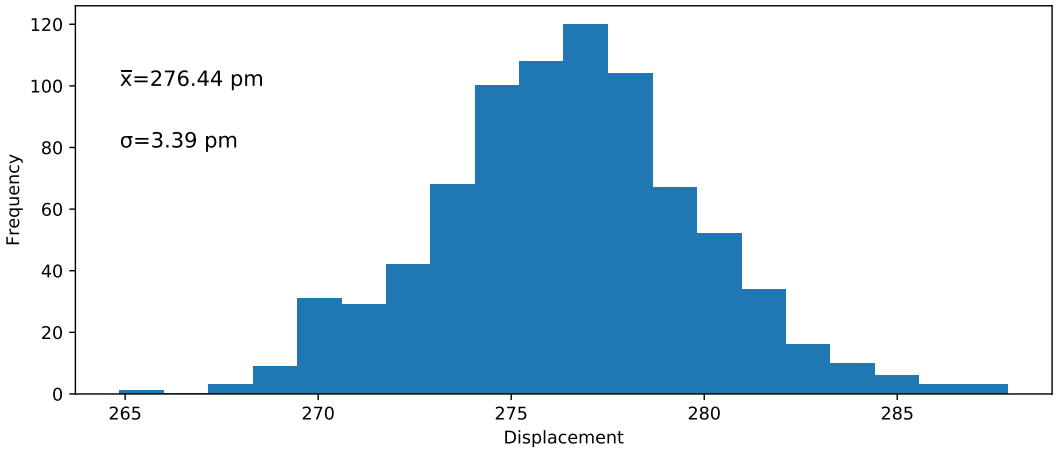

Figure 3.2: Histogram of REVSTEM precision. Because the scan direction is in all four directions, the Sr-Ti/O distances do not need to be split up by angle.

3.3 Simulations with Added Noise

Another possible limitation on improving precision could be the signal-to-noise ratio of a registered image. In order to test this, I created artificial 1024 x 1024 pixel HAADF images with perfect Gaussians that mimicked my experimental data with respect to atomic column positions and relative intensities. Sr atomic columns had a maximum brightness of 1, Ti/O atomic columns had a maximum brightness of 0.6, and the background of the images was 0. I then created the noise to add on to the image by creating a separate 1024 x 1024 pixel image where each pixel was a random value sampled from a uniform distribution from 0 to 1 [8]. I then multiplied this noise-filled image by different factors, n, varying from 0 to 2, and then added each of these new noise images to a copy of the original simulated HAADF image. Each new 1024 x 1024 data set would be a simulated HAADF image with a signal-to-noise ratio of $\frac{1}{n}$. Finally, I analyzed these simulated images by determining their centers using the MOG code and comparing the uncertainty in MOG fitting to the precision of the Sr-Ti/O distances. Zoomed-in portions of these simulations are shown in Fig. 3.3.

In reality, the noise in an experimental image is Gaussian in nature. Therefore, to be more accurate, the noise added to each pixel in a simulation should be sam-

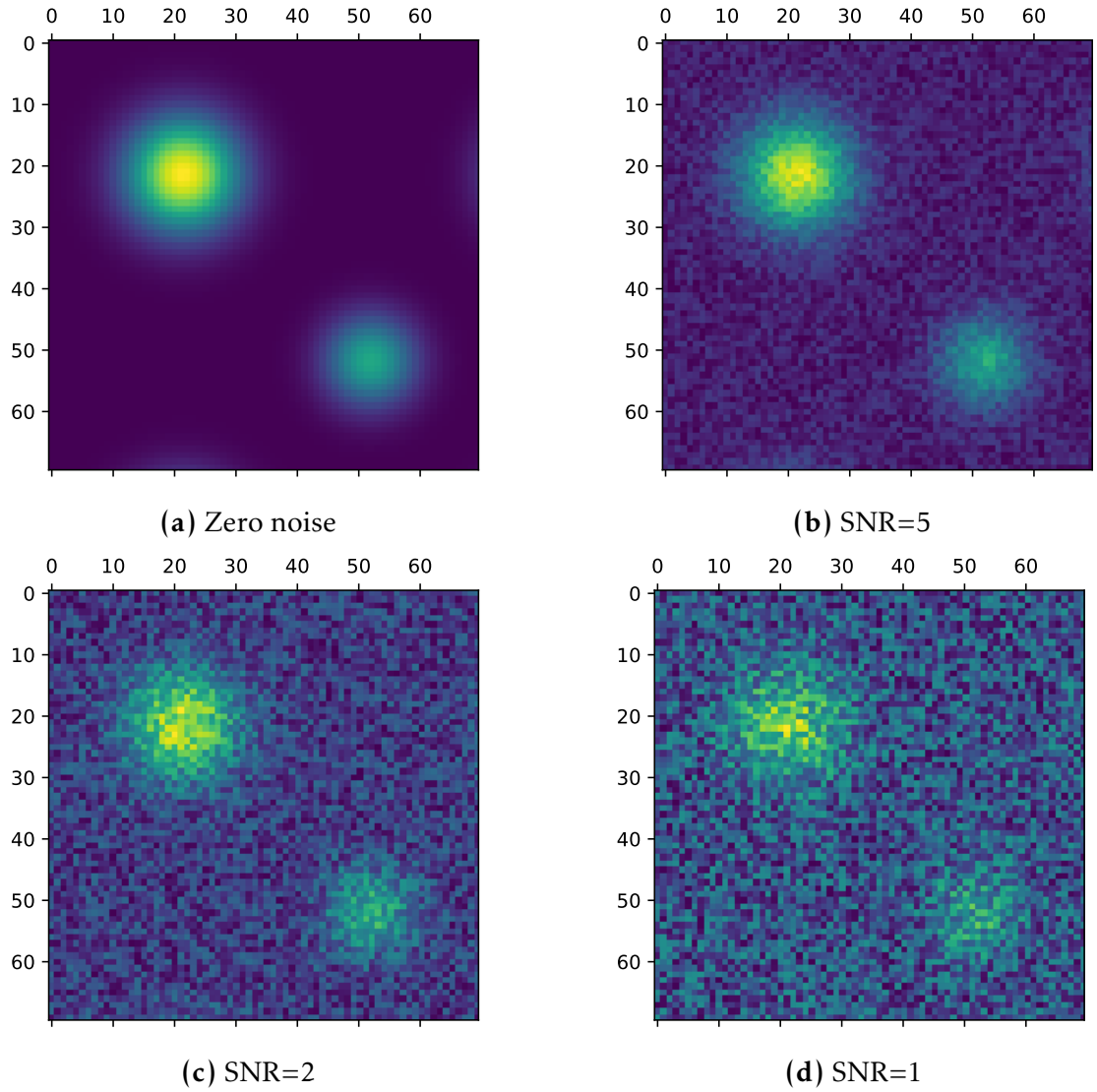

(a) Zero noise

(b) SNR=5

(c) SNR=2

(d) SNR=1

Figure 3.3: Cropped HAADF-STEM simulations with varying signal-to-noise ratios (SNR). Artificial 1024 x 1024 images were made with perfect Gaussians that mimic the position and relative brightness of atomic columns in experimental HAADF-STEM registered images. Each simulation was then added to a 1024 x 1024 noise matrix filled with values randomly sampled from 1 to n, where $\frac{1}{n}$ is the desired signal-to-noise of the image.

pled from a Gaussian distribution instead of a uniform distribution. However, this most likely would not alter my results significantly because it most likely would not affect the MOG fitting or atomic column distance measurements.

Here, the MOG uncertainty for each atomic column is the uncertainty for x and y added in quadrature $\left(\sigma_{Sr} = \sqrt{\sigma_{x_{Sr}}^2 + \sigma_{y_{Sr}}^2}\right.$ and $\left.\sigma_{Ti} = \sqrt{\sigma_{x_{Ti}}^2 + \sigma_{y_{Ti}}^2}\right)$. My results show that the uncertainty of the MOG fitting to atomic columns worsens as the signal-to-noise ratio is lowered. While this finding was expected, it is interest-

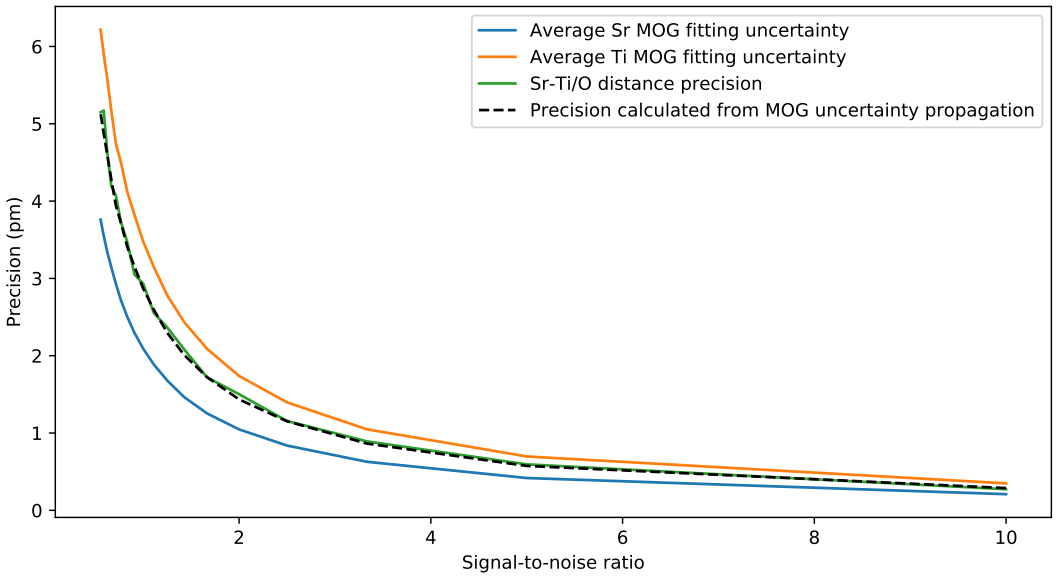

Figure 3.4: Precisions and MOG fitting uncertainties of simulated images with perfect lattice positions and with varying signal-to-noise ratios. Precisions of Sr-Ti/O atomic column distances are closely correlated with the uncertainty in MOG fitting because there is no distribution in the distances between atomic columns. When comparing the propagation of error from MOG fitting (black dashed line) to the precision of atomic column distances (green line), the curves are nearly identical.

ing to note that the precision of the entire image (i.e. Sr-Ti/O distances) follows the same trend as the uncertainties of the MOG fitting to Sr and Ti columns, as shown in Fig. 3.4. Because there is no distribution in the distances between atomic columns before adding noise, the precision of Sr-Ti/O atomic column distances is solely dependent upon the propagation of error from the MOG fitting procedure. If the distance between a Sr atomic column and its neighboring Ti/O atomic column is given by

$$d = \sqrt{(\Delta x)^2 + (\Delta y)^2} \tag{3.1}$$

where $\Delta x = x_{Sr} - x_{Ti}$ and $\Delta y = y_{Sr} - y_{Ti}$, then I can use the fundamental theorem of error propagation to find the expected value for σ_d, the precision of Sr-Ti/O atomic column distances.

$$\sigma_d^2 = \sum_i \left(\frac{\partial d}{\partial x_i}\right)^2 \sigma_{x_i}^2 \tag{3.2}$$

$$\sigma_d = \sqrt{\left(\frac{\partial d}{\partial x_{Sr}}\right)^2 \sigma_{x_{Sr}}^2 + \left(\frac{\partial d}{\partial x_{Ti}}\right)^2 \sigma_{x_{Ti}}^2 + \left(\frac{\partial d}{\partial y_{Sr}}\right)^2 \sigma_{y_{Sr}}^2 + \left(\frac{\partial d}{\partial y_{Ti}}\right)^2 \sigma_{y_{Ti}}^2} \tag{3.3}$$

$$\sigma_d = \sqrt{\left(\frac{\Delta x}{d}\right)^2 \sigma_{x_{Sr}}^2 + \left(\frac{\Delta x}{d}\right)^2 \sigma_{x_{Ti}}^2 + \left(\frac{\Delta y}{d}\right)^2 \sigma_{y_{Sr}}^2 + \left(\frac{\Delta y}{d}\right)^2 \sigma_{y_{Ti}}^2} \tag{3.4}$$

Here, $\sigma_{x_{Sr}}$, $\sigma_{x_{Ti}}$, $\sigma_{y_{Sr}}$, and $\sigma_{y_{Ti}}$ are the average uncertainties of MOG fitting to Sr and Ti/O atomic columns in the x and y coordinates. Furthermore, in simulated images, I can approximate $\Delta x \approx \Delta y$, which yields the following relations:

$$\sigma_d \approx \sqrt{\left(\frac{\Delta x}{d}\right)^2 \left(\sigma_{x_{Sr}}^2 + \sigma_{x_{Ti}}^2 + \sigma_{y_{Sr}}^2 + \sigma_{y_{Ti}}^2\right)} \tag{3.5}$$

$$\sigma_d \approx \sqrt{\frac{1}{2}\left(\sigma_{Sr}^2 + \sigma_{Ti}^2\right)} \tag{3.6}$$

This again shows that when assuming fixed distances between atoms, the error in their distances is closely related to the error in their Gaussian fitting. I used Eq. 3.6 for each simulated image to calculate the expected precision of atomic column distances due to the propagation of their MOG uncertainties, shown as the black dashed line in Fig. 3.4. This turns out to be nearly identical to the precision calculated from the standard deviation of histograms of Sr-Ti/O distances (green line).

However, my experimental images show precision of Sr-Ti/O distances to be almost ten times larger than the uncertainty of the MOG fitting for each column. This indicates that the majority of experimental uncertainty is most likely not attributed to the signal-to-noise ratio.

3.4 Varying Stack Size

One way that microscopists directly increase the signal-to-noise ratio in HAADF images is by increasing the size of the stack. When correlating multiple fast scans together, it's important to have a large enough stack so as to create a registered

image with enough counts, N, that will give a high enough signal-to-noise ratio. As $N \to \infty$, the precision of an image is expected to go to zero.

Typically, our group uses stacks of 50 for these scan parameters, but here I explore the precision of a registered image with respect to its original stack size, ranging from 5 to 100 images in a stack. The image stack used was a 1024 x 1024 x 0.5 μs/pixel data set with 100 total images in the stack.

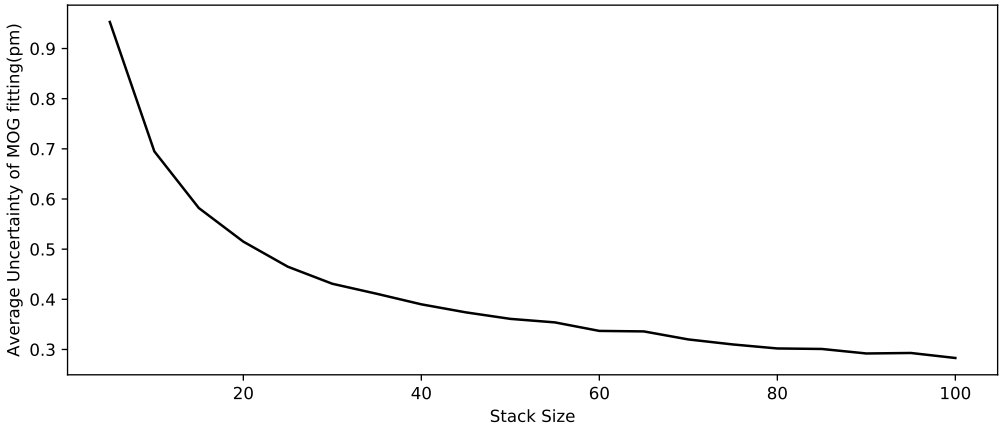

(a) Average uncertainty of MOG fitting for each atomic column, averaged between Sr and Ti. This is essentially how accurate the position of each atomic center is known

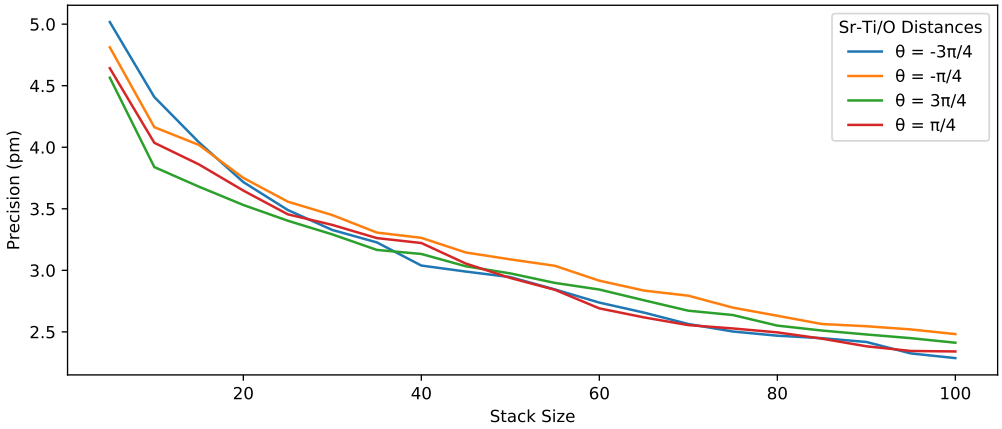

(b) Precision of Sr-Ti/O atomic column distances. Precision is determined by the standard deviation of the distribution of these distances.

Figure 3.5: A 1024 x 1024 x 0.5 μs/pixel HAADF stack shortened to different sizes. Registered images of each stack yield the following precision values. With registering more scans together, the signal-to-noise ratio of an image increases due to an increase in N, the number of counts, which in turn improves the precision of the image.

The results in Fig. 3.5 show that increasing stack size lowers the uncertainty in the MOG fitting for each atomic column. This confirms that correlating more

images leads to a registered image with a higher signal-to-noise ratio, which improves the ability of the MOG to determine the center of the atomic column.

This is also in agreement with my simulation results, showing that an improved MOG fitting leads to an improved precision for measuring atomic column distances. However, it is important to note that the largest possible stack size for this data set gave a MOG fitting uncertainty much below 1 pm, but the precision of the Sr-Ti/O distances still does not go below 2 pm.

I also executed an abbreviated version of this experiment for a 256 x 256 x 2μs/pixel stack with 500 images, since this was the largest stack I obtained. The image that was registered using the shortened stack (only 80 images) had a MOG fitting uncertainty of 1.10 pm, while the image that was registered using the full stack (500 images) had a MOG fitting uncertainty of 0.93 pm. Furthermore, the shortened stack yielded a registered image with precisions of 3.70 pm, 3.61 pm, 3.67 pm, and 3.62 pm for the Sr-Ti/O distances at $3\pi/4$, $\pi/4$, $-\pi/4$, and $-3\pi/4$ respectively. The full stack gave a registered image with respective precisions of 2.92 pm, 2.71 pm, 2.85 pm, and 2.85 pm. The precision of the registered image seems to have improved with increasing the stack size, though not enough to bring it down below 2 pm.

It is possible that even larger stack sizes above could improve the precision further, but it seems that it will level off around 2 or 2.5 pm. This shows that even larger stacks are not able to eliminate the fluctuations in Sr-Ti/O distances.

3.5 Binning vs. Non-binning of Registered Images

In addition to improving the signal-to-noise ratio by increasing the number of scans in a stack, I also inquired as to whether altering an image post-registration could average out noise and increase the precision this way. This is especially important when looking at high magnification images since each atomic column is represented by hundreds of pixels. Here I used a 1024 x 1024 x 0.5 μs/pixel data set, registered with Savitzky's rigid registration code and cropped to be square.

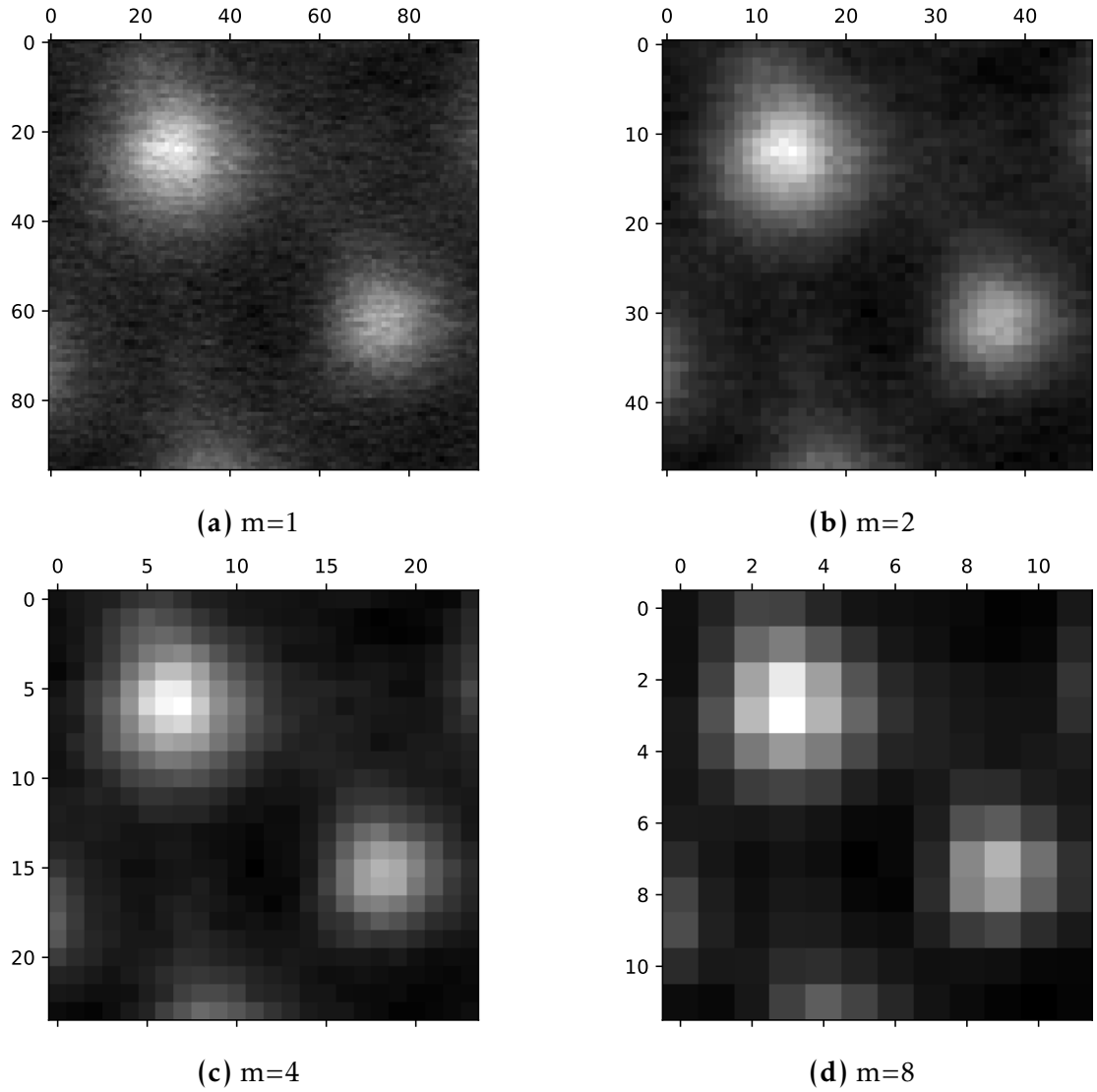

Figure 3.6: Cropped registered HAADF-STEM image of STO with various binning factors. A binning factor of m means that the width of the image in pixels is divided by m. Each pixel in the new binned image is a sum of m^2 pixels from the unbinned image.

In order to rebin an image, the dimensions of the image are divided by some factor (henceforth called the binning factor). For example, if the binning factor is 2, then each pixel in the new rebinned image is a sum of 4 pixels in the unbinned image.

For each binned image, I found the distances between each Sr column to its nearest Sr neighbor, and each Ti/O column to its nearest Ti/O neighbor. I did this rather than measuring Sr-Ti/O distances so as to examine the effects of binning on each column independently. I also separated these by direction (horizontal

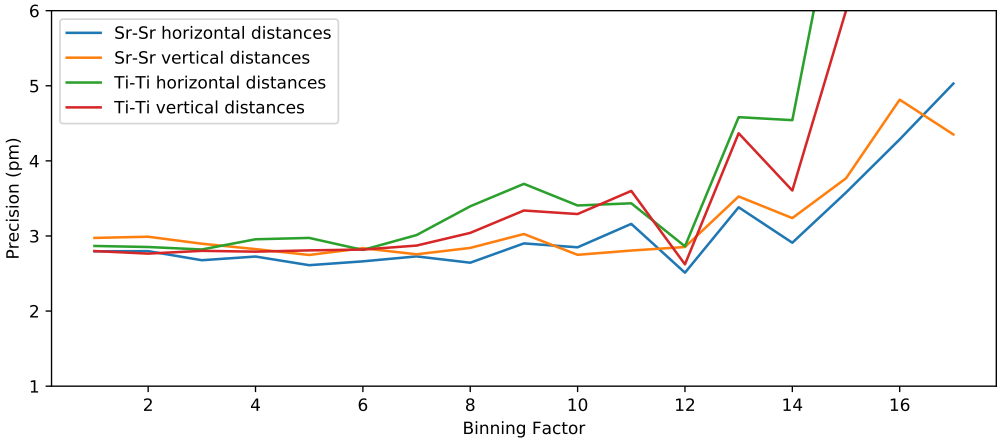

Figure 3.7: Precisions of the binned images. Precisions of atomic column distances don't seem to depend on the binning factor until about m=12.

and vertical) to account for any scan distortions in the horizontal scan direction.

Figure 3.7 shows that low binning factors have no effect on the precision of lattice constant measurements. It is only when the binning factor increases above 12 that the precision is drastically affected. Additionally, the Ti/O-Ti/O precision diverges from the Sr-Sr precision. This is most likely due to the fact that the ratio of atomic column radius to atomic column distances is smaller for Ti/O columns than it is for Sr columns.

From these findings, I conclude that averaging out the noise in each atomic column post-registration has no effect on the precision of the image. This supports my findings from altering the stack size, showing that images with higher signal-to-noise ratios must be limited by some physical phenomena rather than the noise of the image.

3.6 Varying Scan Parameters with Constant Total Scan Time

To find the optimal scan parameters for minimizing precision, I imaged an STO sample under various pixel dwell times and pixel densities. I shortened each stack size so that every stack had the same total scan time (10.5 s) to account for sample drift over the entire scan time. The results are shown in Fig. 3.8. I also show the results for only 1024 x 1024 in Fig. 3.9 to show a more clear trend.

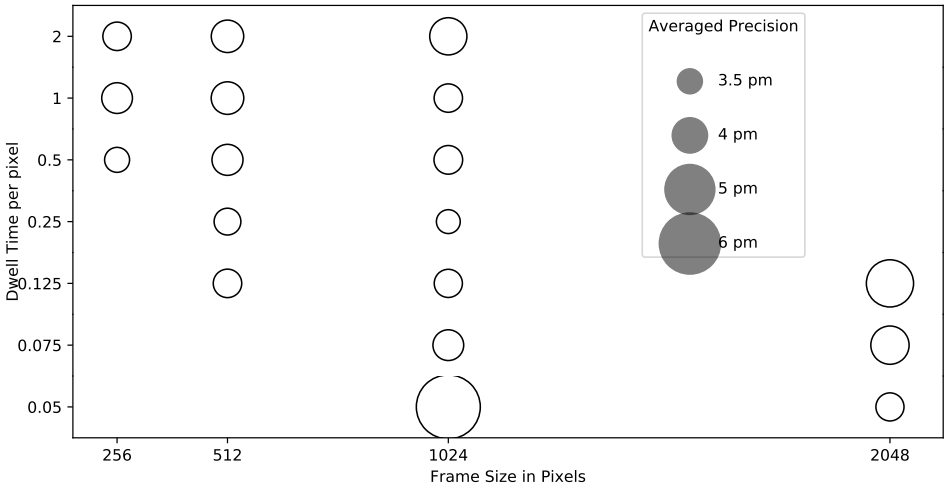

Figure 3.8: Precisions of each image with varying dwell times per pixel and pixel sizes, scaled by area of the circle at each point. Total stack scan time is kept constant for every image at 10.485 s.

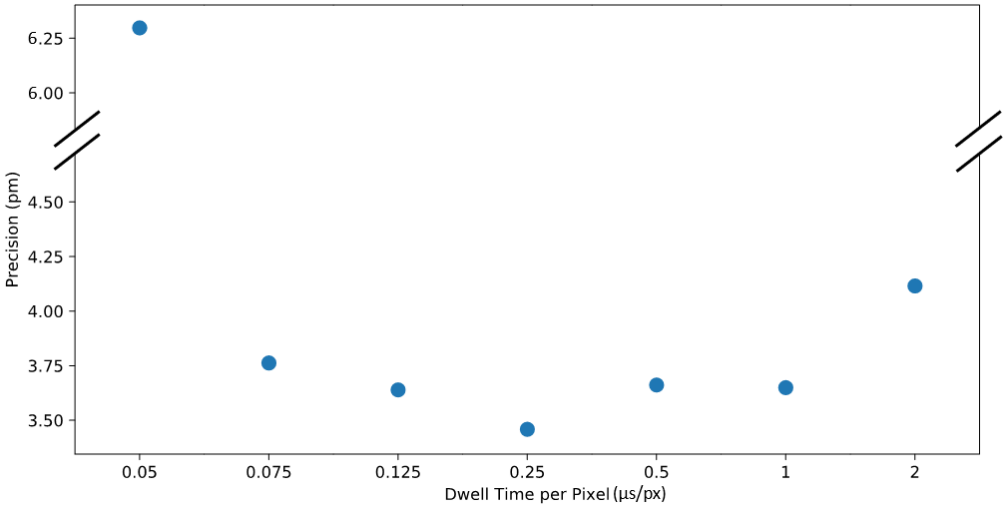

Figure 3.9: Varying Scan parameters for 1024 x 1024 images. A dwell time of 0.25 μs/pixel achieves the best precision with this sample. Shortening the dwell time lowers precision by moving through the field of view too fast, and lengthening the dwell time lowers the precision by allowing for scan distortions.

With 1024 x 1024 scan parameters, it appears that 0.25 μs/pixel dwell times achieve the best precision. If the dwell time is shorter than this, the precision lowers quite drastically, likely because the position of the microscope probe is less reliable when moving quickly throughout the image. This can be seen directly in Fig. 3.10, where images taken at the shortest dwell times have extreme streaking artifacts. Conversely, increasing dwell time to 2 μs/pixel causes a significant

amount of drift in the sample within a single frame, leading to a distortion of the image and a lower value of precision after rigid registration. These images with longer dwell times would most likely require non-rigid registration to correct for scan distortions.

For larger pixel densities such as 2048 x 2048, it appears that the shortest dwell time is optimal because it already takes four times as long to perform a single scan as it does for a 1024 x 1024 image with the same dwell time per pixel. For this frame size, the 0.05 μs/pixel dwell time gives approximately the same frame time as the 1024 x 1024 x 0.25 μs/pixel parameters, which explains why these precisions are the lowest.

The 512 x 512 and 256 x 256 images seem to give worse precision in comparison to 1024 x 1024 images with the same dwell times, but this may be due to a loss in resolution of the image since the field of view is kept constant. However, these two frame sizes are comparable to one another, most likely due to the fact that both are performing very fast scans with very little drift within each frame.

Future experiments would have to be done in order to find an average value of precision among images for each scan parameter. Additionally, shorter dwell times for 256 x 256 and 512 x 512 images were not possible due to a shortage of images in each stack to make a stack with a long total scan time on the order of 10 s. Therefore, taking longer scans at lower pixel densities would be helpful for comparing to larger pixel densities with the same dwell time per pixel.

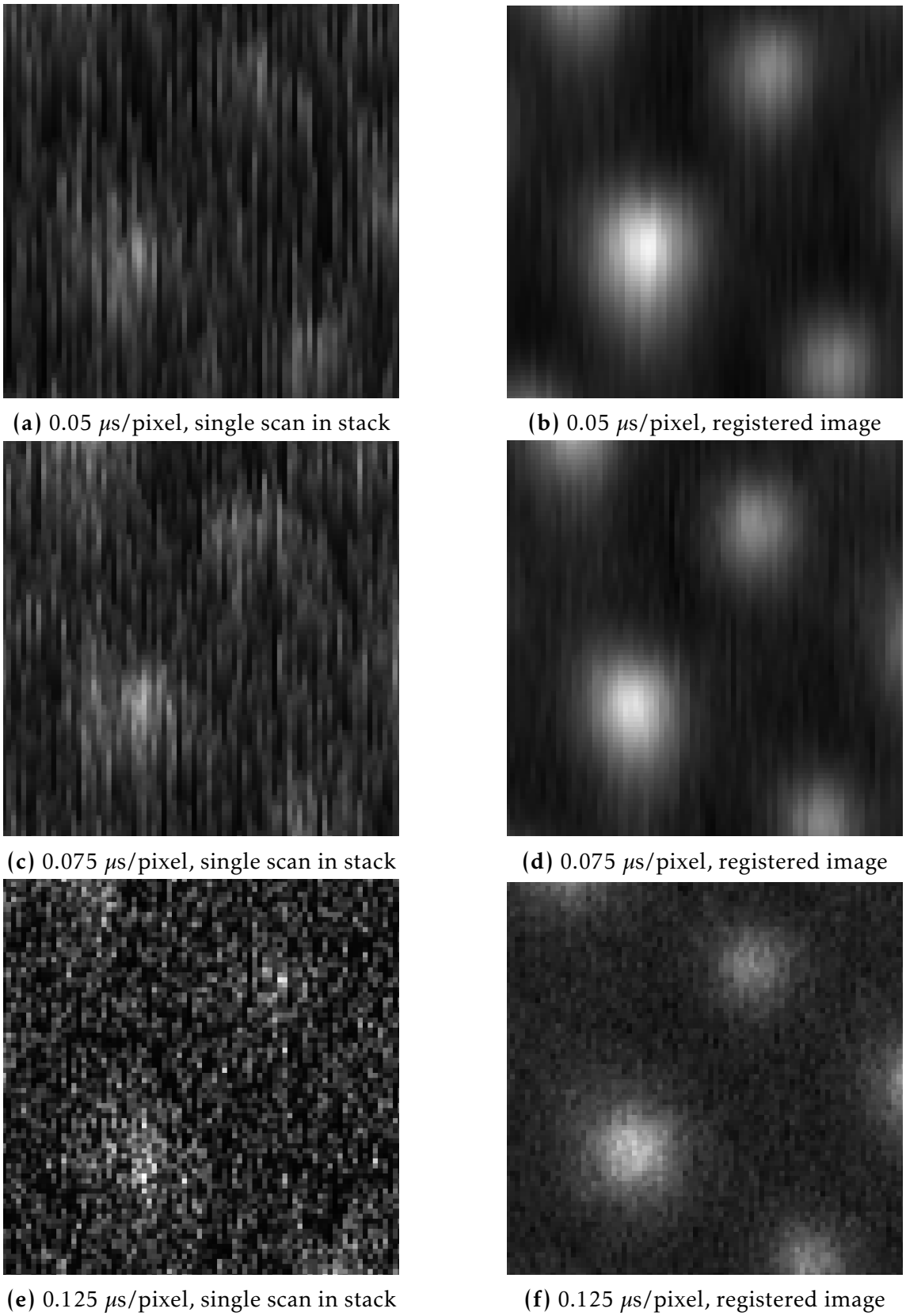

(a) 0.05 μs/pixel, single scan in stack

(b) 0.05 μs/pixel, registered image

(c) 0.075 μs/pixel, single scan in stack

(d) 0.075 μs/pixel, registered image

(e) 0.125 μs/pixel, single scan in stack

(f) 0.125 μs/pixel, registered image

Figure 3.10: Close-up sections of HAADF images with varying dwell times. The shortest dwell times (0.05 and 0.075 μs/pixel) cause streaky images, which could be a major cause in lowering the precision

Chapter 4

Conclusions and Future Work

4.1 Conclusions

I showed that precision, defined by the standard deviation of Sr-Ti/O atomic column distances, for a fast scan HAADF-STEM image of an STO crystal is limited by experimental factors, such as the scan parameters and the number of images in the stack. I demonstrated that increasing the size of the stack improves the signal-to-noise ratio of the image, which in turn improves the Gaussian fitting to each atomic column as well as the overall precision of Sr-Ti/O distances in the image. I also compared scan parameters to find that the best precision came from a stack with 1024 x 1024 x 0.25 μs/pixel scan parameters, though this would need to be confirmed with future experiments.

On the flip side, I found that the method of analyzing the data sets had little to no impact on the precision of the images. For stacks comprised of fast scans, the final precision of the image is neither dependent on the method of registration nor the direction of the scan. Additionally, experimental data with very high signal-to-noise ratios still yielded precisions above 2 pm, whereas simulated data easily showed precisions below 1 pm. Binning the images to average out the noise also did not improve precision.

Therefore, it seems that the precision of HAADF-STEM images of STO is limited not by these analytical methods, but rather by some systematic issue. This could be a systematic error of the microscope setup or physical movements within the lattice.

4.2 Future work

Though none of the experimental data sets shown in this thesis were able to achieve sub-picometer precision, future experiments could be performed at cryogenic temperatures to attempt to improve the precision past this point. Low temperatures would minimize thermal fluctuations, possibly leading to fewer variations in the atomic lattice.

Future experiments could also improve the data shown in Fig. 3.8 by acquiring more data points. Determining the precision for multiple images with the same scan parameters would allow us to confidently say which scan parameters are optimal for improving precision.

Bibliography

[1] S. Van Aert et al. "Optimal experimental design of STEM measurement of atom column positions". In: *Ultramicroscopy* 90 (2002), pp. 273–289.

[2] Ismail El Baggari et al. "Nature and evolution of incommensurate charge order in manganites visualized with cryogenic scanning transmission electron microscopy". In: *Proceedings of the National Academy of Sciences of the United States of America* 115.7 (2018), pp. 1445–1450.

[3] Sara Bals et al. "Statistical estimation of atomic positions from exit wave reconstruction with a precision in the picometer range". In: *Physical Review Letters* 96.9 (2006).

[4] Benjamin Berkels et al. "Optimized imaging using non-rigid registration". In: *Ultramicroscopy* 138 (2014), pp. 45–56.

[5] "Beyond the diffraction limit". In: *Nature Photonics* 3.361 (2009).

[6] Jie Chen et al. "Single-crystal thin films of cesium lead bromide perovskite epitaxially grown on metal oxide perovskite ($SrTiO_3$)". In: *Journal of the American Chemical Society* 139.38 (2017), pp. 13525–13532.

[7] Colin Clement. *mog - GitLab*. URL: gligible.lassp.cornell.edu/colin/mog.

[8] The Scipy Community. *numpy.random.rand - NumPy v1.16 Manual*. URL: https://docs.scipy.org/doc/numpy/reference/generated/numpy.random.rand.html.

[9] The Scipy Community. *Scipy.spatial.KDTree - SciPy v0.14.0 Reference Guide*. URL: https://docs.scipy.org/doc/scipy-0.14.0/reference/generated/scipy.spatial.KDTree.html.

[10] Photutils Developers. *DAOStarFinder - Photutils v0.6*. URL: https://photutils.readthedocs.io/en/stable/api/photutils.DAOStarFinder.html#photutils.DAOStarFinder.

[11] Photutils Developers. *Photutils: An Astropy Package for Photometry*. URL: https://photutils.readthedocs.io/en/stable/index.html.

[12] S. D. Findlay et al. "Dynamics of annular bright field imaging in scanning transmission electron microscopy". In: *Ultramicroscopy* 110 (2010), pp. 903–923.

[13] Stephen Gasiorowicz. "Quantum Physics". In: 3rd ed. Addison-Wesley, 2003. Chap. 1.4.

[14] Young-Min Kim et al. "Probing oxygen vacancy concentration and homogeneity in solid-oxide fuel-cell cathode materials on the subunit-cell level". In: *Nature Materials* 11.7 (2012), pp. 888–894.

[15] Koji Kimoto et al. "Local crystal structure analysis with several picometer precision using scanning transmission electron microscopy". In: *Ultramicroscopy* 110 (2010), pp. 778–782.

[16] Kelvin Li. *Harvard Science Review: A History of Microscopy*. URL: https://harvardsciencereview.com/2017/12/15/a-history-of-microscopy/.

[17] Xiahan Sang and James M. LeBeau. "Revolving scanning transmission electron microscopy: Correcting sample drift distortion without prior knowledge". In: *Ulltramicroscopy* 138 (2014), pp. 28–35.

[18] Benjamin H. Savitzky et al. "Bending and breaking of stripes in a charge ordered manganite". In: *Nature Communications* 8.1883 (2017).

[19] Benjamin H. Savitzky et al. "Image registration of low signal-to-noise cryo-STEM data". In: *Ultramicroscopy* 191 (2018), pp. 56–65.

[20] Kristof Szot et al. “Influence of dislocations in transition metal oxides on selected physical and chemical properties”. In: *Crystals* 8.24 (2018).

[21] Yu-Xin Tong, Qing-Hua Zhang, and Lin Gu. “Scanning transmission electron microscopy: A review of high angle annular dark field and annular bright field imaging and applications in lithium-ion batteries”. In: *Chinese Physics* 27.6 (2018).

[22] Andrew B. Yankovich et al. “Picometre-precision analysis of scanning transmission electron microscopy images of platinum nanocatalysts”. In: *Nature Communications* 5.4155 (2014).

[23] Dan Zhou et al. “Sample tilt effects on atom column position determination in ABF–STEM imaging”. In: *Ultramicroscopy* 160 (2016), pp. 110–117.

[24] Barbara Zitová and Jan Flusser. “Image registration methods: a survey”. In: *Image and Vision Computing* 21.4 (2003), pp. 977–1000.